Peer-reviewed version available at *Energies* **2020**, *13*, 1296; doi:10.3390/en13061296

Article

Single-diode models of PV modules: a comparison of conventional approaches and proposal of a novel model

Tuyen Nguyen-Duc [1,†,‡]*, Huy Nguyen-Duc [1,‡], Thinh Le-Viet [1,‡] and Hirotaka Takano [2,]

[1] Power System Department, Hanoi University of Science and Technology
[2] Department of Electrical, Electronic and Computer Engineering, Gifu University
* Correspondence: tuyen.nguyenduc@hust.edu.vn; Tel.: +81-986-509-059 (VietNam)

Received: date; Accepted: date; Published: date

Abstract: In this paper, the seven traditional models of Photovoltaic (PV) modules are reviewed comprehensively to find out the appropriate model to be reliable. All the models are validated using the Matlab code and made a graphical comparison. The accuracy and convergence of each model are evaluated using data of manufactured PV panels. Then, a novel model is proposed showing its consistent performance. The three most key parameters of single-diode model are self-revised to adapt to various type of PV modules. This new method is verified in three types of PV panels' data measured by National Renewable Energy Laboratory (NREL), US. The validated data show promising results when the error RMSEs' range of the proposed model is under 0.36.

Keywords: Single-diode model, Five-parameter model, Photovoltaic panels, Analytics method

Nomenclature

a	diode ideality factor [-]
a_{ref}	diode ideality factor at the Standard Test Condition (STC) [-]
a_{max}	maximum value of diode ideality factor [-]
E_{gap}	bandgap energy of the semiconductor material [J]
G	solar irradiance [W/m^2]
G_{ref}	solar irradiance at the STC: 1000 [W/m^2]
I	current generated by the PV modules [A]
I_d	Shockley diode current [A]
I_{mpp}	current at the maximum power point (MPP) [A]
I_{pv}	photovoltaic current [A]
$I_{pv,ref}$	photovoltaic current at the STC [A]
I_{sat}	reverse saturation current [A]
I_{sc}	short-circuit current [A]
$I_{sc,ref}$	short-circuit current at the STC [A]
$I_{sc}(G,T)$	short-circuit current at other cell temperature (T)- solar irradiance (G) conditions (T-G conditions) [A]
k	Boltzmann constant: 1.381×10^{-23}[J/K]
K_i	thermal coefficient of the short-circuit current [A/^{o}C]
K_v	thermal coefficient of the open-circuit voltage [V/^{o}C]
N_s	number of series-connected cells [-]
P	power of the PV module [W]
$P_{max,e}$	experimental maximum power of the panel [W]
q	electron charge: $1.60217646 \times 10^{-19}$[C]
R_{sh}	shunt resistance [Ω]
$R_{sh,min}$	minimum shunt resistance [Ω]
$R_{sh}(G,T)$	shunt resistance at other levels of the cell temperature and solar irradiance [Ω]
R_{sho}	reciprocal of the slope of the current-voltage (I-V) characteristic of the panel for $V = 0$ and $I = I_{sc}$ [Ω]
R_s	series resistance [Ω]
$R_s(G,T)$	series resistance at other levels of the cell temperature and solar irradiance [Ω]
R_{so}	reciprocal of the slope of the I-V characteristic of the panel for $V = V_{oc}$ and $I = 0$ [Ω]
tol_p	the pre-defined tolerance of maximum power at the STC [-]
T_{ref}	temperature at the STC: 298.15 [K]
T	cell temperature [K]
V	voltage generated by the PV modules [V]
V_{mpp}	voltage at the MPP [V]
V_{oc}	open-circuit voltage [V]
$V_{oc}(G,T)$	open-circuit voltage at other T-G conditions [V]
V_t	thermal voltage of the diode [V]

1. Introduction

The rapid exhaustion of conventional energy resources, such as coal, crude oil, and natural gas, have been threating to energy security in the world. Since the renewable resources are clean and inexhaustible, the penetration of renewable energy has been arising from time to time in academia, industry, business, and government. Concerning 100% renewable goal in the next few decades worldwide, renewable energy has been becoming a hot topic in the research community. In this context, Photovoltaic (PV) energy becomes one of the prominent renewable energy resources. With the increase of more than 30% in 2018, the power generation from PV is estimated to over 580 TWh [1]. Because of the technical improvements in PV and the dramatic drop in the price of solar PV panels, solar PV systems continue developing. In terms of generation, by 2050, solar PV would become the second-largest power generation source, just behind the wind power. This growth would meet 25% of the total energy demand globally [2]. To estimate the economic feasibility of a solar PV system, the evaluation of the output power of a PV plant need to be addressed. Identifying the

standard I-V characteristics of specific PV panels is a key to estimate accurately the output power of PV panels. As a result, the amount of research has proposed various methods to predict the performance of a PV module based on modeling it, all of which can be divided into analytical methods and metaheuristic algorithms[3]. Some optimization techniques are employed in metaheuristic algorithms, have been applied to obtain the model parameters as follows: simulated annealing [4], bacterial foraging algorithm[5], genetic algorithm [6], differential evolution [7], partial algorithm[8], artificial bee colony[9], simplified swarm optimization[10], etc. Although these models impose no restrictions on the problem formulation[11], metaheuristic algorithms might take long computational time and convergence difficulty. Meanwhile, in [11–26,29–35], analytics methods utilize a set of mathematical equations and assumptions from the datasheet provided by manufacturers. The trade-off between model accuracy and computational time makes the analytics methods much popular in engineering applications than metaheuristic methods.

The best way to analyze the behavior of the PV generator is to adopt an equivalent circuit and to analyze relevant equations describing it [14]. A PV cell is described by an equivalent circuit consisting of a current source, at least one diode, and one resistor [15] based on the intrinsic characteristics. The single-diode model (SDM) [13,16,17] and the double-diode model [11,18,19] have gained the most researchers' attentions, specifically the SDM. Although the double-diode model has a certain advantage, that is representing the recombination loss in the depletion region [20], the double-diode model requires solving an implicit nonlinear seven-parameters[11]. This has led to more difficulties in the calculation of the initial values, long computational time, and algorithm complexity. Meanwhile, the SDM gets the desired compromise between accuracy and simplicity [20].

Different methods have been proposed to extract five parameters of the SDM. In [12–21], a set of implicit equations accompanied by assumptions and simplifications were used to formulate the equations obtaining the model parameters.

An iterative and analytical method are conducted by [13,17,22], which proposed a method to estimate parameters through a trial-and-error approach.

Meanwhile, model parameters were identified by using mathematical manipulations in [14,15,23–26]. Specifically, Lambert-W function at five experimental points was applied in [14,15,24–26].

Refs. [3,27,28] reviewed the remarkable models from 2002 to 2017. The comparisons among models were discussed to choose the model fitting the applications in reality. However, all models are only investigated their performances on one type of PV module. Consequently, the selection of a suitable model for an application is decided just based on computational time and model accuracy, which is insufficient to assess properties of various type of PV panels. In this article, we conduct experiments on three main types of PV modules under varied solar irradiance and cell temperature, such the performance of a PV system largely depends on the cell temperature (T)- solar irradiance (G) conditions (T-G)[17]. Since the new method has proved its advantages, it is verified in three types of PV panels, whose data are experimented by National Renewable Energy Laboratory (NREL), USA. Since the results have shown the promise of this method, it could be used to apply in predicting the performance of a PV panel.

The main contributions of this paper are four folded:

- Review previous models to build I-V curves of PV modules
- Compare the accuracy of these models
- Propose a higher performance model
- Validate the proposed model by real PV module's data

The rest of this paper is organized as follows. Section 2 briefly introduces the fundamental model of the SDM. Section 3 describes reviewed models. Section 4 discusses on the reviewed model and then Section 5 describes proposed model. Section 6 shows the numerical results validating the reviewed and proposed models. Finally, the conclusion is drawn in Section 7.

Preprints (www.preprints.org) | NOT PEER-REVIEWED | Posted: 5 March 2020 doi:10.20944/preprints202003.0084.v1

Peer-reviewed version available at Energies 2020, 13, 1296; doi:10.3390/en13061296

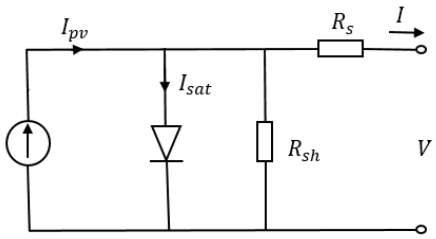

Figure 1. Equivalent circuit of SDM for PV cells

2. Equivalent circuit of the Single-Diode Model

Figure 1 illustrates the well-known equivalent circuit of the SDM, which consists of one current source, one diode, one series resistor, and one shunt resistor. The series resistor is added to take into account the voltage which drops across the transport resistances of the solar cell. The shunt resistor represents the effect of leakage current in the p-n interface of the diode and the edges, as well as the shunt resistance occurring across the solar cell surface[29]. Normally, the estimated value of shunt resistance is very high compared to the series resistance.

The relationship between the output current-voltage is expressed by the following equation:

$$I = I_{pv} - I_d - \frac{V + IR_s}{R_{sh}} \tag{1}$$

I_{pv} is the PV current, generated by electron-hole pairs within a solar cell. I_d is the Shockley diode current, which is described by Eq. 2, where I_{sat} is the reverse saturation current measuring the leakage or recombination of minority carriers across the $p-n$ junction in reverse bias [25], which is calculated by means of Eq. 3. The single diode model assumes that the Shockley current can be described by a single exponential dependence modified by the diode ideality factor a [25]. E_{gap} is the bandgap energy of the semiconductor material (E_{gap}=1.12 eV for the crystalline Si at 25°C [32,33]).

$$I_d = I_{sat}\left(e^{\frac{qV}{akT}} - 1\right) \tag{2}$$

$$I_{sat} = CT^3 e^{\left(-\frac{E_{gap}}{kT}\right)} \tag{3}$$

In fact, PV generators are made of a number of PV cells connected in series and parallel, not referred to as a single PV cell. The operating voltage of the PV cell is few hundreds of millivolts, while the current generates at high irradiance levels is of some amperes. As a result, to reach the desired voltage, a number of connected-series cells are arranged into PV modules. So some researchers have used a modified expression of Eq. 1 as follow:

$$I = I_{pv} - I_{sat}\left(e^{\frac{V}{aN_sV_t}} - 1\right) - \frac{V + IR_s}{R_{sh}} \tag{4}$$

V_t is defined as the thermal voltage of the cell:

$$V_t = \frac{kT}{q} \tag{5}$$

3. Methodology extracting model parameters from datasheet values

All reviewed models use information from the datasheet provided by the manufacturers. Usually, manufacturers provide the values of significant points, i.e. it's short-circuit current (I_{sc}), it's open-circuit voltage (V_{oc}), it's current and voltage at the MPP (I_{mpp}, V_{mpp}), the temperature coefficient of the short-circuit current (K_i), the temperature coefficient of the open-circuit voltage (K_v). Unfortunately,

those values are provided only at the standard test condition (STC). This condition is defined as in the temperature of 25^oC, the irradiance of $1000W/m^2$, and the air mass of 1.5.

In order to estimate effectively the performance of the PV module, the resolution is divided into two steps: estimating five parameters of the SDM model (the ideality factor of diode a, the PV current I_{pv}, the reverse saturation current I_0, the series resistance R_s, the shunt resistance R_{sh}) at the STC, then scaling this model at other T-G conditions of cell temperature and solar irradiance. In these reviewed articles, all methods provide three equations by applying Eq. 4 in the open-circuit, short-circuit, MPP, giving the results:

- At short-circuit point ($I = I_{sc}, V = 0$) :

$$I_{sc} = I_{pv} - I_{sat}\left[\exp\left(\frac{R_s I_{sc}}{aN_s V_t}\right) - 1\right] - \frac{I_{sc}R_s}{R_{sh}} \tag{6}$$

- At open-circuit point ($I = 0, V = V_{oc}$) :

$$0 = I_{pv} - I_{sat}\left[\exp\left(\frac{V_{oc}}{aN_s V_t}\right) - 1\right] - \frac{V_{oc}}{R_{sh}} \tag{7}$$

- At the MPP ($I = I_{mpp}$, $V = V_{mpp}$) :

$$I_{mpp} = I_{pv} - I_{sat}\left[\exp\left(\frac{V_{mpp} + R_s I_{mpp}}{aN_s V_t}\right) - 1\right] - \frac{V_{mpp} + R_s I_{mpp}}{R_{sh}} \tag{8}$$

Three eqs. (6) to (8) are utilized in all reviewed methods. To obtain five model parameters, two additional equations or conditions are required. Since solving five transcendental equations contain the exponential functions and five variables, it can not be solved straight away. Different approaches identifying parameters are presented in seven methods as follows.

3.1. Celik and Acikgoz method-2007

Celik and Acikgoz [16] introduced an analytical method to extract five parameters of the SDM. The authors use two following definitions to estimate the values of the series and shunt resistances:

$$R_{so} = -\left(\frac{dV}{dI}\right)_{V=V_{oc}} \tag{9}$$

$$-\frac{1}{R_{sho}} = \left(\frac{dI}{dV}\right)_{I=I_{sc},V=0} = -\frac{\frac{I_{sat}}{aN_sT}\exp\left(\frac{V_{oc}}{aN_sT}\right) + \frac{1}{R_{sh}}}{1 + R_s\left(\frac{I_{sat}}{aN_sT}\exp\left(\frac{V_{oc}}{aN_sT}\right) + \frac{1}{R_{sh}}\right)} - \frac{1}{R_{sho}} = \left(\frac{dI}{dV}\right)_{I=I_{sc}} \tag{10}$$

Where R_{so} and R_{sho} are the reciprocals of the slopes at the open-circuit point and short-circuit point, respectively. Evaluating the series and shunt resistances is not provided by manufacturers. Since manufacturers do not provide the information to evaluate the series and shunt resistances, these data have to be graphic extracted from the I-V curve in the datasheet that may lead to measurement error affecting the results. After that, the following five equations, eqs. (11) to (15), are proposed to calculate model parameters but do not refer to any explanations about these equations.

$$R_{sh} = R_{sho} \tag{11}$$

$$a = \frac{V_{mpp} + I_{mpp}R_{so} - V_{oc}}{V_t N_s\left[\ln\left(I_{sc} - \frac{V_{mpp}}{R_{sh}} - I_{mpp}\right) - \ln\left(I_{sc} - \frac{V_{oc}}{R_{sh}}\right) + \left(\frac{I_{mpp}}{I_{sc} - \frac{V_{oc}}{R_{sh}}}\right)\right]} \tag{12}$$

$$I_{sat} = \left(I_{sc} - \frac{V_{oc}}{R_{sh}}\right) e^{-\frac{V_{oc}}{aN_s V_t}} \tag{13}$$

$$R_s = R_{so} - \left(\frac{aN_s V_t}{I_{sat}} e^{-\frac{V_{oc}}{aN_s V_t}}\right) \tag{14}$$

$$I_{pv} = I_{sc}\left(1 + \frac{R_s}{R_{sh}}\right) + I_{sat}\left(e^{\frac{I_{sc}R_s}{aN_s V_t}} - 1\right) \tag{15}$$

To scale the model at other temperature-irradiance (T-G) conditions, the values of I_{sc} and V_{oc} are calculated as follows:

$$I_{sc}(G,T) = I_{sc}\frac{G}{G_{ref}} + K_i\left(T - T_{ref}\right) \tag{16}$$

$$V_{oc}(G,T) = V_{oc} + aN_s V_t \ln\left(\frac{G}{G_{ref}}\right) + K_v\left(T - T_{ref}\right) \tag{17}$$

As a result of eqs. (11) to (15), four other parameters, except for R_{sh}, can be calculated at the new T-G condition.

3.2. *Villalva et.al 2009*

An iterative method was used in Villalva et al. method to extract five parameters. The process is started with the initial values of series and shunt resistances as follows :

$$R_s = 0 \tag{18}$$

$$R_{sh} = R_{sh,\min} = \frac{V_{mpp}}{I_{sc} - I_{mpp}} - \frac{V_{oc} - V_{mpp}}{I_{mpp}} \tag{19}$$

This process is stopped until reach the pre-defined tolerance of maximum power (tol_p). Substituting the values of the current, voltage and power at the MPP (I_{mpp},V_{mpp},$P_{max,e}$) on Eq. 8, the shunt resistance can be rewritten by the relationship with series resistance as Eq. 20. This equation is used to update the value of the shunt resistance base on the value of the series resistance for each loop.

$$R_{sh} = \frac{V_{mpp}\left(V_{mpp} + I_{mpp}R_s\right)}{V_{mpp}I_{pv} - V_{mpp}I_{sat}e^{\frac{V_{mpp}+I_{mpp}R_s}{N_s a V_t}} + V_{mpp}I_{sat} - P_{\max,e}} \tag{20}$$

In Eq. 6, the second term is assumed can be neglected since it is too low compared to the PV current[32,33]. Therefore, the PV current and the reverse saturation current are respectively calculated as following equations.

$$I_{pv} = \frac{R_s + R_{sh}}{R_{sh}} I_{sc} \tag{21}$$

$$I_{sat} = \frac{I_{pv} - \frac{V_{oc}}{R_{sh}}}{e^{\frac{V_{oc}}{aN_s V_t}} - 1} \tag{22}$$

In the paper published in 2009 [22], the author chose the initial value of the ideality diode factor equal to 1.3. But in the updated version in 2014 on website of author, a is calculated by equation:

$$a = \frac{K_v - \frac{V_{oc}}{T}}{N_s V_t \left(\frac{K_i}{I_{pv}} - \frac{3}{T} - \frac{E_{gap}}{k.T^2} \right)} \tag{23}$$

3.3. Femia 1 et al.-2012

The value of the shunt resistance is considered so high. By assuming $R_{sh} \rightarrow$ infinity, the last term in Eq. 4 can be neglected. Eq. 4 now becomes:

$$I = I_{pv} - I_{sat} \left[e^{\frac{(V+I.R_s)}{N_s a V_t}} - 1 \right] \tag{24}$$

At the short-circuit condition, Eq. 24 becomes:

$$I_{sc} = I_{pv} - I_{sat} \left(e^{\frac{I_{sc} R_s}{a N_s V_t}} - 1 \right) \tag{25}$$

Since $I_{pv,ref} \gg I_{sat,ref} \left(e^{\frac{I_{sc} R_s}{a N_s V_t}} - 1 \right)$, PV current could be assumed equal to the short-circuit current in the STC:

$$I_{pv,ref} = I_{sc,ref} \tag{26}$$

The diode ideality factor is calculated by means of following equation that is explained in detail in [14].

$$a = \frac{\left(K_v - \frac{V_{oc}}{T} \right)}{N_s V_t \left(\frac{K_i}{I_{pv}} - \frac{3}{T} - \frac{E_{gap}}{kT^2} \right)} \tag{27}$$

The reverse saturation current is calculated by rewritten Eq. 24 under open-circuit condition.

$$I_{sat} = I_{pv} e^{-\frac{V_{oc}}{a N_s V_t}} \tag{28}$$

So that the temperature coefficient C in Eq. 3 can be evaluated as follows:

$$C = \frac{I_{sat}}{T^3 e^{-\frac{E_{gap}}{kT}}} \tag{29}$$

The series resistance can be determined by using the MPP data:

$$I_{mpp} = I_{pv} - I_{sat} \left[e^{\frac{V_{mpp} + I_{mpp} R_s}{a N_s V_t}} - 1 \right] \approx I_{pv} - I_{sat} e^{\frac{V_{mpp} + I_{mpp} R_s}{a N_s V_t}} \tag{30}$$

Substituting Eq. 28 into Eq. 30 yields:

$$I_{mpp} = I_{pv} - I_{pv} \left[e^{\frac{(-V_{oc} + V_{mpp} + R_s I_{mpp})}{a N_s V_t}} \right] \tag{31}$$

Thus the series resistance can be calculated by means of the following equation:

$$R_s = \frac{N_s a V_t \ln \left(1 - \frac{I_{mpp}}{I_{pv}} \right) + V_{oc} - V_{mpp}}{I_{mpp}} \tag{32}$$

All eqs. (26) to (28) and (32) allow calculation of the four values of the unknown parameters (I_{pv} , I_{sat}, a, R_s) in Eq. 4.

Preprints (www.preprints.org) | NOT PEER-REVIEWED | Posted: 5 March 2020 doi:10.20944/preprints202003.0084.v1

Peer-reviewed version available at Energies 2020, 13, 1296; doi:10.3390/en13061296

3.4. Femia 2 et al.-2012

In this method, based on the change of the variable $x = \frac{V_{mpp}+R_s I_{mpp}}{aV_t}$, the series and the shunt resistance can be rewritten as functions of x as follows:

$$R_s = \frac{xaV_t - V_{mpp}}{I_{mpp}}; R_{sh} = \frac{xaV_t}{I_{pv} - I_{mpp} - I_{sat}(e^x - 1)} \tag{33}$$

The slope of the P-V curve at the MPP is equal to zero.

$$\left(\frac{\partial P}{\partial V}\right)_{mpp} = 0 \Rightarrow \left(\frac{\partial (VI)}{\partial V}\right)_{mpp} = 0 \Rightarrow I_{mpp} + V_{mpp}\left(\frac{\partial I}{\partial V}\right)_{mpp} = 0 \tag{34}$$

In Eq. 4 derivating the output current respect to the output voltage under the MPP, giving the following equation:

$$I_{mpp} + V_{mpp}\left(\frac{\partial I}{\partial V}\right)_{mpp} = I_{mpp} - V_{mpp}\frac{\frac{1}{R_{sh}} + \frac{I_{sat}}{aV_t}e^{\frac{V_{mpp}+I_{mpp}R_s}{aV_t}}}{1 + \frac{R_s}{R_{sh}} + \frac{R_s I_{sat}}{aV_t}e^{\frac{V_{mpp}+I_{mpp}R_s}{aV_t}}} = 0 \tag{35}$$

By neglecting the small quantity terms, substituting Eq. 33 into Eq. 35:

$$2V_{mpp}\left(I_{mpp} - I_{pv} - I_{sat}\right) + \left(I_{pv} + I_{sat}\right)aV_t x + I_{sat}e^x\left[-aV_t x + V_{mpp}\left(2 - \frac{V_{mpp}}{aV_t}\right)\right] = 0 \tag{36}$$

Simplifying the first two terms in Eq. 36 gives the following equation, which is a function of x:

$$V_{mpp}\left(2I_{mpp} - I_{pv} - I_{sat}\right) + I_{sat}e^x\left[-aV_t x + V_{mpp}\left(2 - \frac{V_{mpp}}{aV_t}\right)\right] = 0 \tag{37}$$

Based on the means of the Lambert W function, which is the solution of the equation $f(x) = xe^x$, leads to:

$$x = lambertW\left[\frac{V_{mpp}(2I_{mpp} - I_{pv} - I_{sat})e^{\frac{V_{mpp}(V_{mpp}-2aV_t)}{a^2V_t^2}}}{aI_{sat}V_t}\right] + 2\frac{V_{mpp}}{aV_t} - \frac{V_{mpp}^2}{a^2V_t^2} \tag{38}$$

The value obtained by Eq. 38 is substituted in Eq. 33 so that the values of the shunt and series resistances result. Three other parameters can be easily extracted using eqs. (6) to (8).

3.5. Brano et al.-2010

Eq. 4 is written in a different form, which expresses the five parameters' dependency on the solar irradiance and the cell temperature.

$$I(\alpha_G, T) = \alpha_G I_{pv}(T) - I_{sat}(\alpha_G, T)\left(e^{\frac{\alpha_G\left[V+K\left(T-T_{ref}\right)\right]+IR_s}{\alpha_G aN_s T}} - 1\right) - \frac{\alpha_G\left[V + K\left(T - T_{ref}\right)\right] + IR_s}{R_{sh}} \tag{39}$$

where $\alpha_G = \frac{G}{G_{ref}}$. When $G = G_{ref}$ and $T = T_{ref}$, Eq. 39 will become Eq. 4. In order to estimate five parameters at the STC, two equations are used to find R_{sho} and R_{so}. With five non-linear equations, an iterative method was used to find five parameters. This procedure is started with two approximations: $I_{pv,ref} = I_{sc,ref}$ and $R_{sh} = R_{sho}$

After initializing a and R_s, three other parameters I_o, I_{pv},and R_{sh} are estimated based on eqs. (6), (8) and (40). After that, a is recalculated by Eq. 7 until satisfying the pre-defined tolerance. Then, R_s is

evaluated by means of Eq. 41. This double process is repeated until both of R_s and a reach the desired accuracies.

$$\left(\frac{dI}{dV}\right)_{I=0,V=V_{oc}} = -\frac{1}{R_{so}} = -\frac{\frac{I_{sat}}{aN_sT}\exp\left(\frac{V_{oc}}{aN_sT}\right)+\frac{1}{R_{sh}}}{1+R_s\left(\frac{I_{sat}}{aN_sT}\exp\left(\frac{V_{oc}}{aN_sT}\right)+\frac{1}{R_{sh}}\right)} \tag{40}$$

$$\left(\frac{dI}{dV}\right)_{I=I_{sc},V=0} = -\frac{1}{R_{sho}} = -\frac{\frac{I_{sat}}{aN_sT}\exp\left(\frac{V_{oc}}{aN_sT}\right)+\frac{1}{R_{sh}}}{1+R_s\left(\frac{I_{sat}}{aN_sT}\exp\left(\frac{V_{oc}}{aN_sT}\right)+\frac{1}{R_{sh}}\right)} \tag{41}$$

In other T-G conditions, the reverse saturation current I_{sat} can be calculated by using the relationships:

$$I_{sat}\left(\alpha_G,T\right) = \alpha_G\left(\frac{I_{pv}\left(T\right)-\frac{V_{oc}(\alpha_G,T)}{R_{sh}}}{e^{\frac{V_{oc}(\alpha_G,T)}{aN_sT}}-1}\right) \tag{42}$$

$I_{sat}\left(\alpha_G,T\right)$ can be approximated by means of:

$$I_{sat}\left(\alpha_G,T\right) = e^{\left(\frac{\alpha_G-0.2}{1-0.2}\right)\ln\frac{I_{sat}(1,T)}{I_{sat}(0.2,T)}+\ln I_{sat}(0.2,T)} \tag{43}$$

3.6. Cubas et.al-2014

Accompanied by three remarkable eqs. (6) to (8), the diode ideality factor is estimated to be the same as one of Villalva et al. method (2009). The last equation to obtain the final parameter is the differentiation of power respect to the voltage at the MPP equal to zero. Based on some simplifications and assumptions, five parameters can be found by the following equations:

$$\frac{aV_tV_{mpp}\left(2I_{mpp}-I_{sc}\right)}{\left(V_{mpp}I_{sc}+V_{oc}\left(I_{mpp}-I_{sc}\right)\right)\left(V_{mpp}-I_{mpp}R_s\right)-aV_t\left(V_{mpp}I_{sc}-V_{oc}I_{mpp}\right)} = \exp\left(\frac{V_{mpp}+I_{mpp}R_s-V_{oc}}{aV_t}\right) \tag{44}$$

$$R_{sh} = \frac{\left(V_{mpp}-I_{mpp}R_s\right)\left(V_{mpp}-R_s\left(I_{sc}-I_{mpp}\right)-aV_t\right)}{\left(V_{mpp}-I_{mpp}R_s\right)\left(I_{sc}-I_{mpp}\right)-aV_tI_{mpp}} \tag{45}$$

$$I_{sat} = \frac{\left(R_{sh}+R_s\right)I_{sc}-V_{oc}}{R_{sh}\exp\left(\frac{V_{oc}}{aV_t}\right)} \tag{46}$$

$$I_{pv} = \frac{R_{sh}+R_s}{R_{sh}}I_{sc} \tag{47}$$

Eq. 44 is an implicit expression of the series resistance. It can be solved by fsolved function in Matlab. The way to scale SDM's parameters at other T-G conditions is not mentioned in Cubas's paper.

3.7. Laudani et.al 2014

In Laudani et.al 2014, five parameters can be classified in two groups: three dependent variables G_{sh}, I_{sat}, and I_{pv} and two independent variables R_s and a. G_{sh}, I_{sat}, and I_{pv} are rewritten as functions of R_s, a

$$G_{sh} = \frac{Exp_{oc}(I_{mpp}-I_{sc})+Exp_{mpp}I_{sc}-Exp_{sc}I_{mpp}}{A_1Exp_{sc}+A_2Exp_{mpp}+A_3Exp_{oc}} \tag{48}$$

$$I_{sat} = \frac{V_{oc}(I_{sc}-I_{mpp})-V_{mpp}I_{sc}}{A_1Exp_{sc}+A_2Exp_{mpp}+A_3Exp_{oc}} \tag{49}$$

$$I_{pv} = \frac{I_{sc}V_{oc}(Exp_{mpp} - 1) + I_{sc}V_{mpp}(1 - Exp_{oc}) + I_{mpp}V_{oc}(1 - Exp_{sc})}{A_1 Exp_{sc} + A_2 Exp_{mpp} + A_3 Exp_{oc}} \quad (50)$$

where $V_t = \frac{kT}{q}$; $Exp_{sc} = \exp\left(\frac{I_{sc}R_s}{N_s a V_t}\right)$; $Exp_{oc} = \exp\left(\frac{V_{oc}}{N_s a V_t}\right)$; $Exp_{mpp} = \exp\left(\frac{V_{mpp}+I_{mpp}R_s}{N_s a V_t}\right)$; $P_1 = V_{mpp}I_{mpp}$; $P_2 = (V_{oc} - V_{mpp})I_{mpp}$; $P_3 = (V_{oc} - V_{mpp})(I_{sc} - I_{mpp})$; $P_4 = V_{mpp}(I_{sc} - I_{mpp})$; $A_1 = V_{mpp} + R_s I_{mpp} - V_{oc}$; $A_2 = V_{oc} - R_s I_{sc}$; $A_3 = R_s I_{sc} - R_s I_{mpp} - V_{mpp}$; $G_{sh} = R^{-1}{}_{sh}$;

The differentiation of power respect to the voltage at the MPP at the STC is used.

$$\frac{I_{mpp}}{V_{mpp}} = \frac{\frac{I_{sat}}{N_s a V_t} Exp_{mpp} + G_{sh}}{1 + \frac{R_s I_{sat}}{N_s a V_t} Exp_{mpp} + G_{sh} R_s} \quad (51)$$

By making some simplifications and substituting eqs. (48) to (50) into Eq. 51, the following condition is formulated:

$$f_1(R_s, a) = (P_2 - P_1)Exp_{sc} + (P_1 - P_4)Exp_{oc} + ((P_1 - P_3)\frac{I_{mpp}R_s - V_{mpp}}{aN_s V_t} + (P_4 - P_2))Exp_{mpp} = 0 \quad (52)$$

By using the Lambert fuction, $R_s^{\max}$ is expressed as a function of a:

$$R_s^{\max}(a) = \frac{V_{mpp}}{I_{mpp}} + \frac{N_s a V_t}{I_{mpp}} \left\{1 + W_{-1}\left[-\exp\left(\frac{V_{oc} - aN_s V_t - 2V_{mpp}}{N_s a V_t}\right)\right]\right\} \quad (53)$$

There is a value of $a_{\max}$, which is defined by the intersection between the R_s curve (by solving f_1) and the $R_s^{\max}$ curve (according to Eq. 53). The authors suggested using the heuristic rule: $a = 0.9 \times a_{\max}$. After finding a, the R_s is computed by numerically solving Eq. 53. As a result, the values of I_{sat}, I_{pv}, R_{sh} are calculated by means of eqs. (6) to (8) starting from R_s and a obtained previously.

4. Discussion on reviewed modules

4.1. Categorize methods

Based on the approaches to obtain the model parameters, seven methods can be categorized into three types that are the analytical method, iterative method, and numerical method. These methods are easy to program in Matlab, using only available data in datasheets from manufacturers. However, each method has advantages and disadvantages.

In Villalva et al. [22] and Brano et al. [17], iterative methods were employed. To start the loop, these methods require to calculate some initial parameters. These values usually are approximately estimated by making assumptions. All assumptions, coupled with initial values for each model, are summarized in Table 1. In the Brano method, finding two initial calculations (R_{so}, R_{sho}) might be difficult since the number of points in the I-V curve chosen to calculate two values has a significant impact on the model's result and model divergence. In Villalva method, the diode ideality factor in Eq. 23 is estimated based on the relationship with bandgap energy, which is unavailable for some PV panels. This equation, therefore, are not applicable to other PV panels, such as CIGS or poly-junction ones. Generally speaking, the iterative method gets the compromise between the algorithm complexity and the model accuracy since it is simpler than the numerical method and more accurate compared to analytical one.

On the other hand, Celik et al.[16], Femia 1[14] and Cubas[24] used the analytical method, posing a set of assumptions to formulate equations to calculate model parameters. These equations usually can be solved straight away, reducing the calculation time. However, since they come with assumptions to simplify equations, the model accuracy also reduces. Assumptions are listed in Table 1.

When numerical method comes into play, mathematical functions are introduced to solve the dependent relationship between current output and voltage output, specifically Lambert-W function

Table 1. Comparison among reviewed models

	Method	Assumptions (A) Intial guesses (IG), Initial Caculations (IC)	a	R_s	R_{sh}
Celik	Analytical	IC:R_{so}, R_{sho} A: $R_{sh} = R_{sho}$	$f(R_{so}, R_{sho})$ (Eq.12)	Self-revised (Eq. 14)	Self-revised (Eq.11)
Villalva	Iterative	IG:tol_P, $R_s = 0$ $R_p = R_{p,\min} = \frac{V_{mp}}{I_{sc}-I_{mp}} - \frac{V_{oc}-V_{mp}}{I_{mp}}$ A: $I_{pv,ref} \gg I_{sat,ref}\left[\exp\left(\frac{IR_s}{aN_sV_t}\right) - 1\right]$	Constant (Eq.23)	Self-revised (Iterative)	Self-revised (Iterative)
Femia 1	Analytical	A: $R_sh = \infty$ $I_{pv,ref} \gg I_{sat,ref}\left[\exp\left(\frac{IR_s}{aN_sV_t}\right) - 1\right]$	Constant (Eq.23)	Constant (Eq.32)	Constant ($R_sh = \infty$)
Femia 2	Numerical	A:$R_s I_{mpp,ref} \ll 2V_{mpp,ref}$	Constant (Eq.23)	Constant	Constant
Brano	Iterative	A:$e^{V_{oc}/aN_sVt} \gg 1$, $R_s \ll R_p$, $I_{pv} \approx I_{sc}$ $\frac{I_{sat}}{aN_sV_t}e^{\frac{I_{sc}R_s}{aN_sV_t}} \ll \frac{1}{R_p} \ll \frac{I_{sat}}{aN_sV_t}e^{\frac{V_{oc}}{aN_sV_t}}$ IC:R_{so}, R_{po} IG:$R_s = R_{so}, R_p = R_{po}, a = 1$	Self-revised (Iterative)	Self-revised (Iterative)	Self-revised (Iterative)
Cubas	Analytical	IG: a A: $I_{pv,ref} \gg I_{sat,ref}\left[\exp\left(\frac{IR_s}{aN_sV_t}\right) - 1\right]$	Constant (initial choice)	Const (Eq. 44)	Const (Eq. 45)
Laudani	Numerical	IG: $a = 0.9 \times a_{\max}$	Constant (initial choice)	Const (Eq. 53)	Const (Eq. 8)

in [14,34]. Because the SDM applied numerical method is solved without any assumptions thus they are more accurate at the expense of calculational time.

4.2. When changing from one to another type of PV panel

One thing that should be considered when applying these methods in applications is how effective they are when changing from one to another type of PV panel. Theory speaking, since each characteristic of the PV cell is different, the model parameters consequently change. The series, shunt resistances, and diode ideality factors are considered to manipulate the model [35]. Two other parameters, the reverse saturation current and the PV current, are assumed to be dependent on the three aforementioned parameters. Because the approach of each method is different, thus the model performance also is impacted. In Celik et al. [16] and Brano et al. [17], the diode ideality factor is incorporated in each loop, which fine-tunes the model precision. Two initial calculations, eqs. (11) and (14), are taken into account the resistances of the model for other kinds of PV cells. In this way, the model performance is more effective for each type of PV panel. However, calculating eqs. (11) and (14), as mentioned above, has to choose the number of points of the I-V characteristic. Therefore, these calculations might lead to algorithm divergence when applying for some types of PV panel.

In Cubas et al. [24] and Laudani et al. [34] method, the diode idealty factor is guessed at first. The series and shunt resistances are calculated by specific equations, which can not self-revised when changing from one to another PV panel type. Femia et al.-1 and Femia et al.-2 [14] introduce an equation estimating the diode ideality factor based on the bandgap energy of PV panel material, which is not available for some types of PV panels. As a result, these values have to be predicted in programming.

In Villalva et al. [22], by updating the value of series and shunt resistances after a loop, these values are utilized to fit model performance compared to the provided one. The diode ideality factor is suggested measuring as same as Femia et al.-1 and Femia et al.-2 [14] method, which is unable when the material of PV panel is not silicon crystalline.

Peer-reviewed version available at Energies 2020, 13, 1296; doi:10.3390/en13061296

5. Proposed method

Herein, we propose an iterative method, which takes into account the change of model parameters when changing PV panel type and does not require any initial calculations. Since the second term in Eq. 6 can be neglected [32,33], the PV current is rewritten as:

$$I_{pv} = I_{sc}\frac{R_s + R_{sh}}{R_{sh}} \tag{54}$$

By substituting Eq. 54 into Eq. 8, the shunt resistance can be expressed as a function of the series resistance as in:

$$R_{sh} = \frac{I_{sc}R_s - V_{mpp} - I_{mpp}R_s}{I_{mpp} + I_{sat}\left[\exp\left(\frac{V_{mpp}+I_{mpp}R_s}{aN_sV_t}\right) - 1\right] - I_{sc}} \tag{55}$$

From Eq. 55, the maximum value of the series resistance is calculated by assuming the denominator of the right side of Eq. 55 is zero. So, it is expressed by the following equation:

$$R_{s,\max} = \frac{aV_t \ln\left(\frac{I_{sc}-I_{mpp}}{I_{sat}} - 1\right) - V_{mpp}}{I_{mpp}} \tag{56}$$

$$P_{\max,e} = V_{mpp}I_{mpp} = V_{mpp}\left(I_{pv} - I_{sat}\left[\exp\left(\frac{V_{mpp} + I_{mpp}R_s}{aN_sV_t}\right) - 1\right]\right) - \frac{V_{mpp} + R_sI_{mpp}}{R_{sh}} \tag{57}$$

Although Eq. 55, can be used as a way to update the value of the shunt resistance for each loop, it contains the simplified Eq. 54, contributing the model error. By rearranging Eq. 57, the shunt resistance can be calculated by alternative way as in Eq. 58:

$$R_{sh} = f(R_s) = \frac{V_{mpp}\left(V_{mpp} + I_{mpp}R_s\right)}{V_{mpp}I_{pv} - V_{mpp}I_{sat}\exp\left[\frac{\left(V_{mpp}+I_{mpp}R_s\right)}{aN_sV_t}\right] + V_{mpp}I_{sat} - P_{max,e}} \tag{58}$$

The iterative process starts by $R_s = 0; R_{sh} = f(R_s)$. After that, the PV current can be calculated from Eq. 54, by rearranging Eq. 6.

$$I_{pv} = \frac{R_s + R_{sh}}{R_{sh}}I_{sc} + I_{sat}\left[\exp\left(\frac{R_sI}{aN_sV_t}\right) - 1\right] \tag{59}$$

From Eq. 8, the diode ideality factor is calculated by means of Eq. 60. Finally, the reverse saturation current is calculated by Eq. 61.

$$a_n = \frac{V_{mpp} + I_{mpp}R_s}{V_t \log\left(\frac{I_{pv} - I_{mpp} - \frac{V_{mpp}+I_{mpp}R_s}{R_{sh}}}{I_{sat}} + 1\right)} \tag{60}$$

$$I_{sat} = \frac{I_{pv} - \frac{V_{oc}}{R_{sh}}}{e^{\frac{V_{oc}}{aN_sV_t}} - 1} \tag{61}$$

This process is continued with the value of the series resistance ranging from $[0; R_{s,\max}]$. For each of the value of series resistance, four other parameters will be calculated respectively by eqs. (54), (55), (60) and (61).

To improve the certainty of the algorithm, it is necessary to determine a stopping condition, which does not require any initial guess. For two points in the P-V curve, one is on the left side, and another is on the right side, there is a five-parameter respectively. When substituting this five-parameter into

Preprints (www.preprints.org) | NOT PEER-REVIEWED | Posted: 5 March 2020 doi:10.20944/preprints202003.0084.v1

Peer-reviewed version available at Energies 2020, 13, 1296; doi:10.3390/en13061296

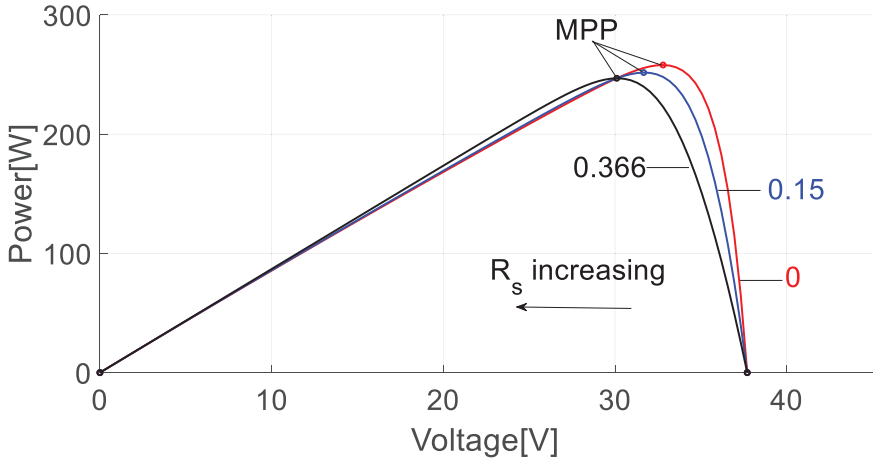

Figure 2. P-V curves plotted for different values of R_s

Eq. 62, which expressed the slope of the P-V curve, this value with respect to the point at the left side is greater than zero and for the point at the right side would be smaller than zero.

$$\frac{dP}{dV} = \frac{d(VI)}{dV} = I + V\frac{dI}{dV} = I - V\frac{\frac{I_{sat}}{aN_sV_t}\exp\left(\frac{V+IR_s}{aN_sV_t}\right) + \frac{1}{R_{sh}}}{1 + \frac{R_sI_{sat}}{aN_sV_t}\exp\left(\frac{V+IR_s}{aN_sV_t}\right) + \frac{R_s}{R_{sh}}} \tag{62}$$

As can be seen in Fig. 2, when the series resistance increases, the peak of the P-V curve will shift from the right side of this fixed point to the left side. Consequently, the derivative of the power with respect to the voltage, as expressed in Eq. 62, will monotonically decrease from the positive to negative. As a result, the process stops until the condition Eq. 63 is satisfied.

$$\left(\frac{dP}{dV}\right)_i\left(\frac{dP}{dV}\right)_{i-1} < 0 \tag{63}$$

Using the interpolation method, the value of R_s is calculated as Eq. 64.

$$R_s = R_{s,i} + (R_{s,i} - R_{s,i-1})\frac{\frac{dP}{dV_{i-1}}}{\frac{dP}{dV_{i-1}} - \frac{dP}{dV_i}} \tag{64}$$

where i is the number of point, in which derivative of the power with respect to the voltage is greater than zero. From Eq. 64, eqs. (54), (55), (60) and (61) five model parameters are identified.

Finally, the procedure is described by a flowchart in Fig. 3.

Since PV systems operate at other T-G conditions further from the STC in reality, it is needed to scale the SDM at other weather conditions. However, only some reviewed methods proposed the way to scale model at operation conditions. In the original papers, only Brano et al. in 2010 [17] and Celik et al. in 2007 [16] proposed the way to scale model at other T-G conditions other than the STC. But in Celik model [16], the authors just estimated only two values of the open-circuit voltage and short-circuit current, using eqs. (15) and (16). Since some datasheets do not provide the coefficient of the MPP, the current and voltage at the MPP can not be scaled, which also means the diode ideality factor can not be estimated. In this case, five eqs. (11) to (15) are unable to scale model. So the method to scale model in [30] is defaulted for all models to verify model parameters at other weather conditions. The series and shunt resistance are considered to vary in inverse linear mode with solar irradiance, as expressed in eqs. (65) and (66). The diode ideality factor is assumed unchanged from its value at the STC. Two remaining parameters, I_{sat} and I_{pv}, are estimated by eqs. (61) and (68). Since all methods use

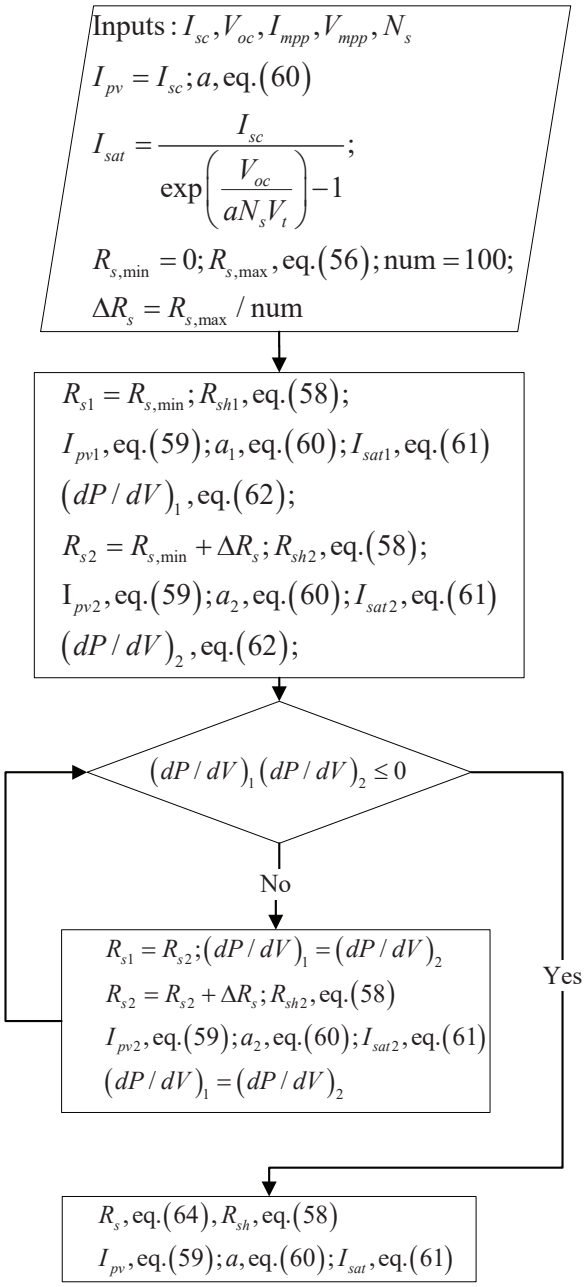

Figure 3. The flowchart to obtain model parameters

one way to scale the models at other levels of the solar irradiance and the cell temperature, the model parameters at the STC has a significant impact on the model performance at these conditions.

$$R_s(G,T) = R_{s,ref}\frac{G_{ref}}{G} \tag{65}$$

$$R_{sh}(G,T) = R_{sh,ref}\frac{G_{ref}}{G} \tag{66}$$

$$a = a_{ref} \tag{67}$$

$$I_{pv} = \left[I_{pv,ref} + K_i\left(T - T_{ref}\right)\right]\frac{G}{G_{ref}} \tag{68}$$

Table 2. Data for evaluating the model parameters of Shell SQ150-PC, Kyocera 175GHT-2 and Sanyo HIT 240HDE4 at the STC

Cell Type	V_{oc}[V]	I_{sc}[A]	V_{mpp}[V]	I_{mpp}[A]	N_s[-]	K_v [V/^{o}C]	K_i [A/^{o}C]
Shell SQ150-PC	43.46	4.82	33.73	4.48	72	-0.161	0.0014
Kyocera 175GHT-2	28.56	8.09	7.47	23.71	48	-0.107	0.00222
Sanyo HIT-240HDE4	43.88	7.4	35.15	7.05	60	-0.109	0.00221

6. Numerical Results

6.1. Investigated models

In this article, seven reviewed models and proposed one are investigated exhaustively on monocrystalline (Shell SQ150-PC), multicrystalline (Kyocera 175GHT-2) and heterojunction (Sanyo HIT 240HDE4) PV modules. For each of PV cell type, seven methods are implemented in the conditions, whose cell temperature and solar irradiance varies.

Table 2 presents data for evaluating the model parameters provided by manufacturers only at the STC. These data are slightly different from the tabular data provided by manufacturers in datasheet because it is graphically extracted from the characteristic voltage-current (I-V)curves in the datasheet.

6.2. Accuracy Validation

All models are verified their performances by both metric forms and graphs. A set of graphs are depicted to validate the models' precisions. Besides, for each graph, all results regarding performance metric of model are reported. The performance metric, namely the root mean squared error (RMSE), is defined as follows:

$$RMSE = \sqrt{\frac{1}{i}\sum_{1}^{i}(I_{m,i} - I_{e,i})^2} \tag{69}$$

where $I_{m,i}$ and $I_{e,i}$ are the measured current values of the model, and the actual current values, respectively, and i is the total number of I-V pairs in the experimental and measured I-V curves.

6.3. Models performances

Figure 4 depicts the I-V characteristic curves, including the curves provided by manufacturers and eight estimated curves of monocrystalline Shell SQ150-PC PV panel at various levels of solar irradiance and cell temperatures, respectively. The data show that eight estimated curves highly agree with the original curves. In Fig. 4.a), all curves are almost overlapped, meanwhile in Fig. 4.c) there is still a little inaccuracy after the bends of curves.

For detailed information, Fig. 4.b) and Fig. 4.d) report the RMSE between individual methods in two cases, ranging solar irradiance and ranging cell temperature. In Fig. 4.b), from 200 W/m^2 to 800W/m^2, Laudani's method reaches the highest accuracy, with the RMSEs range from 0.011 to 0.041. Meanwhile, Celik's method has the lowest accuracy, with the RMSEs range from 0.029 to 0.080. Although the Laudani's method has the highest accuracy when scaling at other conditions, at the STC, its RMSE is greater than Cubas's and proposal's, which indicates its drawback when applying in the STC. One another remarkable point should be taken into account is the accuracies of all methods increase when applying at other levels of cell temperature and solar irradiance. The reason being that when applying eqs. (16) and (17) to scale the open-circuit voltage and the short-circuit current returns the diverge results, so we employ graphic values extracted from the curves in datasheet instead. Fig. 4.d) shows the exactnesses of eight methods at the solar irradiance of $G = 1000$W/m^2 and cell temperature ranging from 20^{o}C to 60^{o}C . As can be seen in Fig. 4.d), Cubas's method shows the best

Preprints (www.preprints.org) | NOT PEER-REVIEWED | Posted: 5 March 2020 doi:10.20944/preprints202003.0084.v1

Peer-reviewed version available at Energies 2020, 13, 1296; doi:10.3390/en13061296

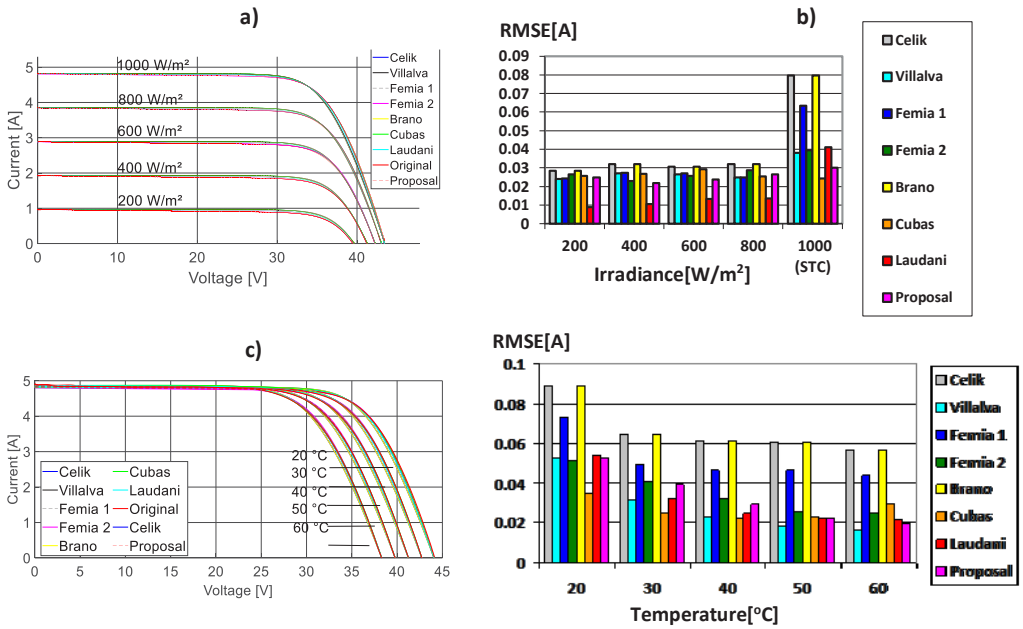

Figure 4. Comparison between calculated (8 models) and maker I-V curves of Shell SQ150-PC: a) at T=25°C; b)RMSE at T=25°C; c) at G=1000[W/m^2]; d) RMSE at G=1000[W/m^2]

performance compared to other methods, with the RMSEs range from 0.016 to 0.053. From 20°C to 40°C, Cubas's method is the most accurate method and Celik's method and Brano's method are the least accurate ones. Although at 50°C and 60°C the RMSEs of Cubas's method are higher than the RMSEs of the proposed method, Villalva's, Femia 2's, and Laudani's, the differences are not large. The effectiveness of model increases from 20°C to 60°C.

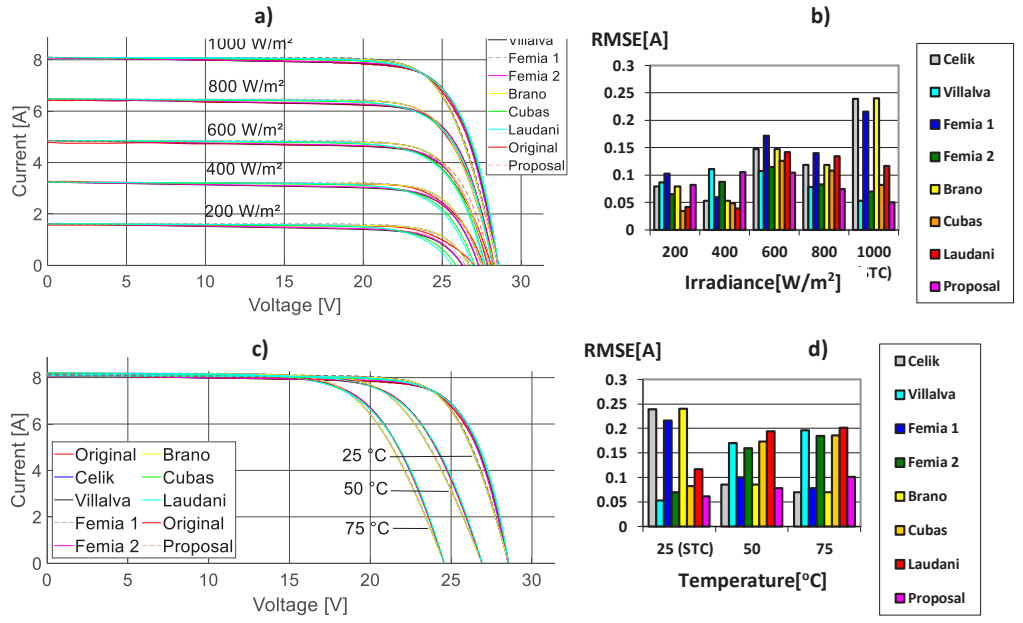

Figure 5. Comparison between calculated (8 models) and maker I-V curves of Kyocera KC175GHT-2:a) at T=25°C; b)RMSE at T=25°C; c) at G=1000[W/m^2]; d) RMSE at G=1000[W/m^2]

For Kyocera KC175GHT-2 PV panel, Fig.5.a) illustrates the precisions of methods at 25°C and various levels of solar irradiance. In Fig.5.a), all of the predicted curves highly agree with the issued ones. Meanwhile, the estimated curves and issued curves at 1000 W/m^2 and various levels of cell temperature are plotted Fig.5.c). In Fig.5.c), some disagreements still happen after the MPP when applying some methods to obtain parameters of the SDM.

As can be seen in Fig. 5.b), at high levels of solar irradiance (1000W/m^2, 800W/m^2 and 600W/m^2) the proposed model has the lowest RMSEs. However, at lower levels of solar irradiance (200W/m^2 and 400W/m^2) the Cubas's model and the Laudani's model have the best accuracy. In Fig. 5.c), generally speaking, after the MPP, eight estimated curves have agreements from the maker curves at the MPP area. As observed in Fig. 5.d), although Villalva's model has the lowest errors at the STC, it's errors are high at 50°C and 75°C. The proposed model shows high accuracy when RMSEs range from 0.06 to 0.1. Since the proposal's model has low and stable RMSEs at various cell temperatures, it shows the effectiveness when scaling in other levels of cell temperature.

Fig. 6 represents performances of the SDM applied eight methods on Sanyo HIT-240HDE4 PV panel. In Fig. 6.a), all reviewed models show a large disagreement compared to original curve at MPP area. This might be explained by the difference in property of this type of PV panel. In order to improve the exactness of model, in proposed method, the value of diode ideality factor is modified. The data in Fig. 6.a) shows the effectiveness of proposed model compared to others.

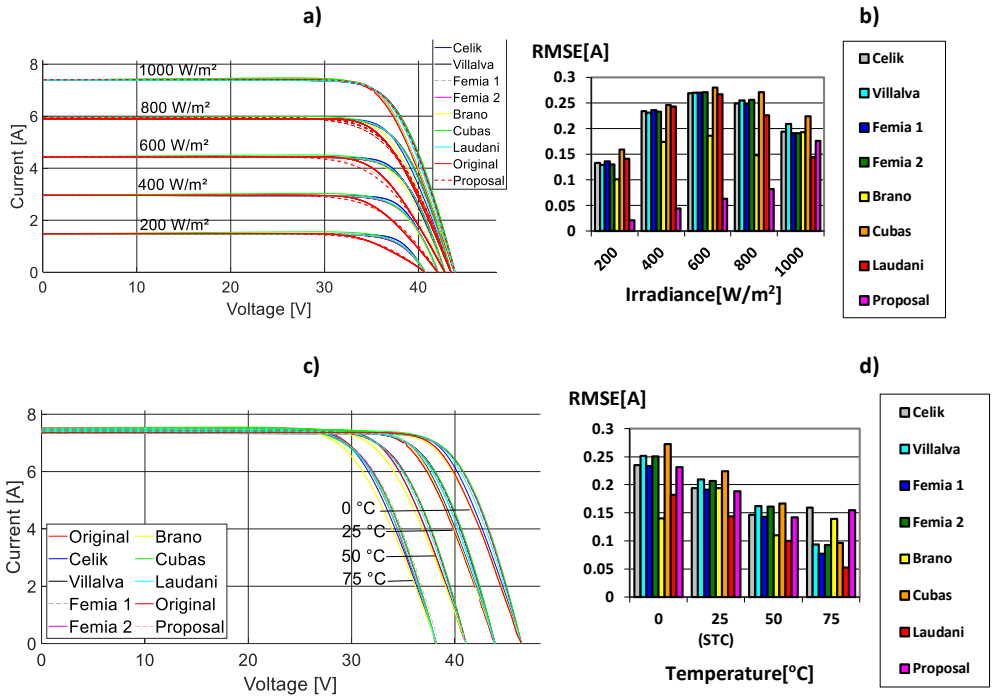

Figure 6. Comparison between calculated (8 models) and issued I-V curves of Sanyo HIT-240HDE4: a) at T=25°C; b)RMSE at T=25°C; c) at G=1000[W/m^2]; d) RMSE at G=1000[W/m^2]

As in single-crystalline and multi-crystalline PV cells, when applying eight methods to obtain I-V curves of Sanyo HIT-240HDE4 at $G = 1000$W/m^2 and cell temperature ranges from 0°C to 75°C, some methods show inaccuracies after the MPP, as reported in Fig. 6.c).

In Fig. 6.b), the proposal shows the best performance since the RMSEs range from 0.021 to 0.176. Although at the STC, the RMSE of proposed method is a bit higher than the RMSE of Laudani's method, its RMSEs are lower compared to RMSEs of other methods at other levels of solar irradiance.

As can be seen from Fig. 6.d), Laudani's method achieves the best performance at 25°C, 50°C, 75°C since the RMSEs range from 0.053 to 0.144. At 0°C, the Brano's method reaches highest accuracy.

This can be explained by applying eqs. (9) and (10) returns values of R_{so} and R_{sho}, which lead to divergence of algorithm. So we suggest a couple value of (R_{so}, R_{sho}) to execute the algorithm of this method.

Shortly, when applying eight methods to identify parameters of the SDM on three types of PV panel, there is not the best model that can achieve the highest accuracy in all conditions. Since the RMSEs of reviewed models range drastically when the levels of solar irradiance and cell temperature change, they have some drawbacks. Although the proposed model does not reach the highest accuracy in all conditions, the difference between its RMSE and the best method's RMSE in each condition is not large. In addition, its RMSEs are more stable, which indicates its high reliability. Therefore, an investigation is conducted to validate the performance of proposed model with the measured data.

6.4. Experimental validation of proposal model

In order to verify the performance of the proposed model at operation conditions, an experiment is conducted on three types of PV panels, that are single-crystalline silicon Cocoa xSi12922, multi-crystalline silicon Cocoa mSi0166, and amorphous crystalline (HIT) Cocoa HIT05667. This experiment is conducted at Cocoa, Floria, US by NREL. The data is available at NREL website [36]. Since the cell temperature does not change much, the solar irradiance has the most significant impact on the model performance. The estimated curves are performed in the following cases:

- **Single-crystalline silicon PV panel**

  As can be seen in Fig. 7, for single-crystalline silicon Cocoa xSi12922 PV panel, the predicted curves have high agreements with the actual curves. At high levels of solar irradiance and cell temperature (G=603.8W/m^2; T=24.8^{o}C to G = 1030.2 W/m^2; T=33.3^{o}C), the proposal curves overestimate the output currents. On the other hand, at lower levels of solar irradiance and cell temperature (G=35.3W/m^2; T=18.9 ^{o}C to G=459.9W/m^2; T=29.5^{o}C), the proposal curves underestimate the output currents.

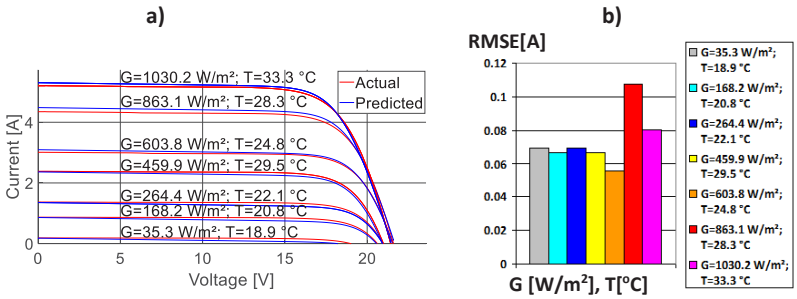

Figure 7. Comparison between the calculated (proposed model) and experimental curves of operation conditions of single-crystalline Cocoa xSi12922 PV panel

- **Multi-crystalline silicon PV panel**

  For multi-crystalline silicon Cocoa mSi0166 PV panel in Fig. 8, the model underestimates the current output. At low levels of solar irradiance and cell temperature, the disagreements between predicted curves and issued curves are larger, which can be explained by the uncertainties of experimental data tend to bigger at low levels of T-G conditions. The predicted curves at high solar irradiance (867.2 W/m^2 and 1030.8 W/m^2) have inaccuracies with actual ones.
- **HIT**

  For amorphous silicon (HIT) Cocoa HIT05667 PV panel in Fig. 9, there are disagreements between estimated curves and issued curves, and especially it tends to extend after the MPP.

  In figs. 7 and 8, the RMSEs of the model are lowest at irradiances (400W/m^2 to 600W/m^2) and highest at 800W/m^2 to 1000W/m^2 . There are two reasons for this tendency. The effectiveness

Preprints (www.preprints.org) | NOT PEER-REVIEWED | Posted: 5 March 2020 doi:10.20944/preprints202003.0084.v1

Peer-reviewed version available at Energies 2020, 13, 1296; doi:10.3390/en13061296

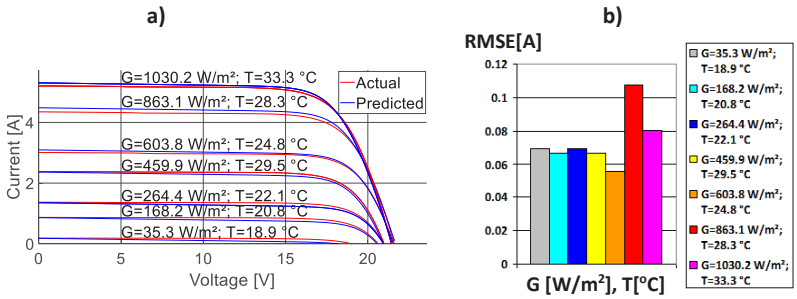

Figure 8. Comparison between the calculated (proposed model) and experimental curves of operation conditions of multi-crystalline Cocoa mSi0166 PV panel

of the SDM applying the proposed method is significantly effected by applying two eqs. (16) and (17). Consequently, in figs. 7 to 9, the SDM shows more inaccuracies in open-circuit voltage. The RMSEs of the SDM at the solar irradiance from 30W/m^2 to 270W/m^2 is higher than it's counterpart at the solar irradiance from 400W/m^2 to 600W/m^2 because the uncertainty of measuring instruments is higher when measuring at low levels of solar irradiance.

As can be seen in Fig. 9, the RMSEs are smaller at low levels of solar irradiance and cell temperature. The RMSEs tend to be higher at high levels of solar irradiance (635.1 W/m^2 to 1031.3 W/m^2) when they range from 0.2 to 0.3. At low levels of solar irradiance (35.5 W/m^2 to 1687 W/m^2) the RMSEs are lower with the RMSEs range from 0.05 to 0.1.

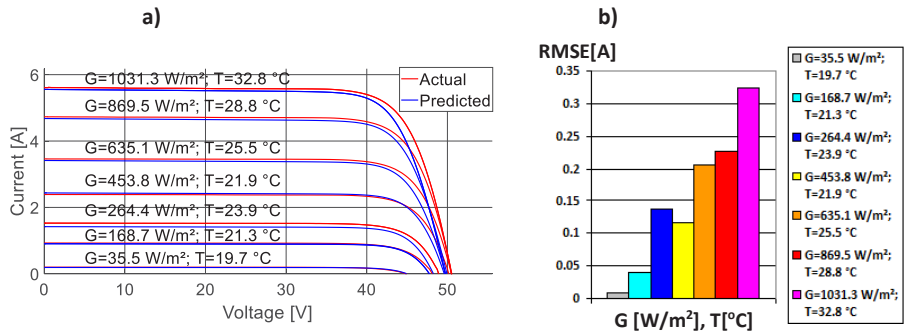

Figure 9. Comparison between the calculated (proposed model) and experimental curves of operation conditions of amorphous silicon Cocoa HIT05667 PV panel

The tendency of RMSEs in figs. 7 and 8 is not as same as in Fig. 9 because in HIT PV panel, the fill factor is different from two aforementioned PV types. The error of eqs. (16) and (17) contributing to the SDM error surpass the error of the uncertainty of measurement at low levels of solar irradiance.

In the above investigation, the model is tested by fixed levels of solar irradiance and cell temperature and various value of the external load, R_L. For given values of solar irradiance, cell temperature and external load, the I-V characteristics of PV panels depicted by present the function $I = f(V)$ and the external load characteristic $I = V/R_L$ [17]. To make more comprehensive validation, the proposed method is implemented for particular T-G conditions and constant values of external load, which are characterized by 3000 pairs of (T, G). Fig. 10 performs the predicted points and actual points for Cocoa xSi12922 PV panel, Cocoa mSi0166 PV panel, Cocoa HIT05667 PV panel respectively. The data show that the proposed method underestimates the output current for three types of panel. In addition, the simulation results tend to be more precise at lower values T and G. The RMSE is 0.3544, 0.25 and 0.2888 for Cocoa xSi12922 PV panel, Cocoa mSi0166 PV panel, Cocoa HIT05667 PV panel respectively.

Four remarkable values, that are the open-circuit point voltage, the short-circuit current, the voltage and current at the MPP, play the main role in obtaining the SDM as they provide the input for solving three main eqs. (6) to (8). In fact, expressions like eqs. (16) and (17) can not achieve the desired model precision. In addition, the coefficient of maximum power is not provided in datasheets of some PV types, thus the voltage and current at the MPP can not be scaled. So, the SDM can not be solved as at the STC, instead of a set of eqs. (61) and (65) to (68) are used to scaled for each model parameter. This way might lead to the uncertainty of methods and reduce model accuracy.

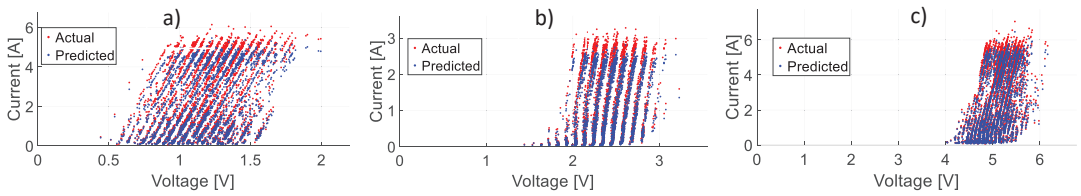

Figure 10. The actual and simulated points of: a) Cocoa xSi12922 PV panel, b) Cocoa mSi0166 PV panel, c) Cocoa HIT05667 PV panel

7. Conclusion

In this article, seven methods of identifying parameters using the SDM have been reviewed and discussed comprehensively. The advantages and disadvantages of each method are analyzed. Although some methods present good results in estimating the I-V curves in some cases, their reliability is not high when changing to other types of PV panels. A new method is proposed, which shows consistent performance for all investigated PV panels under various conditions of cell temperature and solar irradiance. This new method is verified in three types of PV panels, which are measured by NREL, US. For three types of PV panels, single-crystalline silicon, multi-crystalline silicon, and amorphous silicon, the experimental results show that the RMSEs below 0.36. This error is an acceptable tolerance in practical applications requiring high accuracies such as PV power forecast and MPPT. Accurate I-V characteristics of PV panels contribute to the success in forecasting the maximum power point in the MPPT algorithm and the output power in PV power forecast.

Author Contributions: Nguyen Duc Tuyen, Nguyen Duc Huy, Le Viet Thinh and Hirokata Takano conceived of the methodology. Nguyen Duc Tuyen and Le Viet Thinh developed the theory and performed the computations. Nguyen Duc Tuyen led the research efforts and led the preparation of this paper. All authors provided critical feedback and helped shape the research, analysis and manuscript. Besides, all authors discussed the results and contributed to the final manuscript.

Funding: This work was funded by Hanoi University of Science and Technology grant number T2018-PC-058

References

1. IEA, “Tracking Power", *Paris* **2019**, https://www.iea.org/reports/tracking-power-2019.
2. IRENA, “Future of Solar Photovoltaic: Deployment, investment, technology, grid integration and socio-economic aspects (A Global Energy Transformation: paper)", *International Renewable Energy Agency* **2019**, Abu Dhabi.
3. Bader S, Ma X and Oelmann B, “One-diode photovoltaic model parameters at indoor illumination levels – A comparison", *Sol. Energy* **2019**, 180, pp.707—16.
4. El-Naggar K M, AlRashidi M R, AlHajri M F and Al-Othman A K, “Simulated Annealing algorithm for photovoltaic parameters identification", *Sol. Energy* **2012** 86(1), pp.266—74.
5. Krishnakumar N, Venugopalan R and Rajasekar N, “Bacterial foraging algorithm based parameter estimation of solar PV model", *Annu. Int. Conf. Emerg. Res. Areas, AICERA and 2013 Int. Conf. Microelectron. Commun. Renew. Energy, ICMiCR 2013 - Proc.*, **2013**.
6. Zagrouba M, Sellami A, Bouaïcha M and Ksouri M, “Identification of PV solar cells and modules parameters using the genetic algorithms: Application to maximum power extraction", *Sol. Energy* **2010** 84(5) pp.860—6.

7. Ishaque K and Salam Z, "An improved modeling method to determine the model parameters of photovoltaic (PV) modules using differential evolution (DE)", *Sol. Energy***2011** 85(9), pp.2349-–59.
8. Khanna V, Das B K, Bisht D, Vandana and Singh P K, "A three diode model for industrial solar cells and estimation of solar cell parameters using PSO algorithm", *Renew. Energy* **2015** 78, pp.105—13.
9. Oliva D, Cuevas E and Pajares G, "Parameter identification of solar cells using artificial bee colony optimization", *Energy* **2014** 72, 93—102.
10. Lin P, Cheng S, Yeh W, Chen Z and Wu L, "Parameters extraction of solar cell models using a modified simplified swarm optimization algorithm", *Sol. Energy* **2017** 144, pp.594—603.
11. Chen Y, Sun Y and Meng Z, "An improved explicit double-diode model of solar cells: Fitness verification and parameter extraction", *Energy Convers and Manag.* **2018** 169, pp.345—58.
12. De Blas M A, Torres J L, Prieto E and García A, "Selecting a suitable model for characterizing photovoltaic devices", *Renew. Energy***2002** 25(3), 371—80.
13. Wang G, Zhao K, Shi J, Chen W, Zhang H, Yang X and Zhao Y, "An iterative approach for modeling photovoltaic modules without implicit equations", *Appl. Energy* **2017** 202, pp.189-–98.
14. Femia N, Petrone G, Spagnuolo G and Vitelli M, "PV Modeling Power Electronics and Control Techniques for Maximum Energy Harvesting in Photovoltaic Systems", *CRC Press* **2017**, pp.1-–33.
15. Hussein A, "A simple approach to extract the unknown parameters of PV modules", *Turkish J. Electr. Eng. Comput. Sci.* **2017** 25, pp. 4431-–44.
16. Celik A N and Acikgoz N, " Modelling and experimental verification of the operating current of mono-crystalline photovoltaic modules using four- and five-parameter models", *Appl. Energy* **2007** 84(1), pp.1-–15.
17. Lo Brano V, Orioli A, Ciulla G and Di Gangi A, "An improved five-parameter model for photovoltaic modules", *Sol. Energy Mater. Sol. Cells* **2010** 94(8), pp.1358-–70.
18. Gow J A and Manning C D, "Development of a photovoltaic array model for use in power-electronics simulation studies", *IEE Proc. Electr. Power Appl.* **1999** 146(2), pp.193-–200.
19. Dehghanzadeh A, Farahani G and Maboodi M, "A novel approximate explicit double-diode model of solar cells for use in simulation studies", *Renew. Energy* **2017** 103, pp.468-–77.
20. Wang G, Zhao K, Qiu T, Yang X, Zhang Y and Zhao Y, "The error analysis of the reverse saturation current of the diode in the modeling of photovoltaic modules", *Energy* **2016** 115, pp.478—85.
21. Hadj Arab A, Chenlo F and Benghanem M, "Loss-of-load probability of photovoltaic water pumping systems", *Sol. Energy* **2004** 76(6), 713—23.
22. Villalva M.G., Gazoli J.R. and Filho E.R., "Comprehensive approach to modeling and simulation of photovoltaic arrays", *IEEE Trans. Power Electron.*, **2009** 24 pp. 1198–1208.
23. Cubas J, Pindado S and Victoria M, "On the analytical approach for modeling photovoltaic systems behavior", *J. Power Sources* **2014** 247, pp.467—74.
24. F.Ghani and M.Duke, "Numerical determination of parasitic resistances of a solar cell using the Lambert W-function", *Sol. Energy* **2011** 85(9), pp.2386—2394.
25. Jain A and Kapoor A, "Exact analytical solutions of the parameters of real solar cells using Lambert W-function", *Sol. Energy Mater. Sol. Cells* **2004** 81(2), pp.269—77.
26. Ghani F, Duke M and Carson J, "Numerical calculation of series and shunt resistances and diode quality factor of a photovoltaic cell using the Lambert W-function", *Sol. Energy* **2013** 91, pp.422—31.
27. Ciulla G, Lo Brano V, Di Dio V and Cipriani G, "A comparison of different one-diode models for the representation of I-V characteristic of a PV cell", *Renew. Sustain. Energy Rev.* **2014** 32, pp.684—96.
28. Humada A M, Hojabri M, Mekhilef S and Hamada H M, "Solar cell parameters extraction based on single and double-diode models: A review", *Renew. Sustain. Energy Rev.* **2016** 56, pp.494—509.
29. Rusirawan D and Farkas I, "Identification of model parameters of the photovoltaic solar cells", *Energy Procedia* **2014** 57, pp.39-–46.
30. De Soto W, Klein S A and Beckman W A, "Improvement and validation of a model for photovoltaic array performance", *Sol. Energ* **2006** 80(1), pp.78-–88.
31. Walker G, "Evaluating MPPT converter topologies using a matlab PV model", *J. Electr. Electron. Eng.* **2001** 21(1), pp.49—55.
32. Kennerud K L, "Analysis of Performance Degradation in CDS Solar Cells", *IEEE Trans. Aerosp. Electron. Syst. AES-5* **1969**, pp. 912-–7.

33. Rodriguez P, Sera D, Teodorescu R and Rodriguez P, "PV Panel Model Based on Datasheet Values PV panel model based on datasheet values", *IEEE International Symposium on Industrial Electronics* **2014**, pp. 2392—6.
34. Antonino Laudani, Francesco Riganti Fulginei and Alessandro Salvini, "Identification of the one-diode model for photovoltaic modules from datasheet values", *Solar Energy* **2014** 108, pp.432–446.
35. Bana S and Saini R P, "A mathematical modeling framework to evaluate the performance of single diode and double diode based SPV systems", *Energy Reports no. 2* **2016**, 171-–87.
36. Marion W, Anderberg A, Deline C, Glick S, Muller M, Perrin G, Rodriguez J, Rummel S, Terwilliger K and Nrel T J S, "User's Manual for Data for Validating Models for PV Module Performance", *https://www.nrel.gov/docs/fy14osti/61610.pdf*, **2014**.